Homozygous missense mutation L673P in adenylate kinase 7 (AK7) leads to primary male infertility and multiple morphological anomalies of the flagella but not to primary ciliary dyskinesia

Patrick Lorès, Charles Coutton, Elma El Khouri, Laurence Stouvenel, Maelle Givelet, Lucie Thomas, Baptiste Rode, Alain Schmitt, Bruno Louis, Zeinab Sakheli, et al.

Human Molecular Genetics, 2018, Vol. 27, No. 7 1196–1211

doi: 10.1093/hmg/ddy034
Advance Access Publication Date: 22 January 2018
Original Article

ORIGINAL ARTICLE

Homozygous missense mutation L673P in adenylate kinase 7 (AK7) leads to primary male infertility and multiple morphological anomalies of the flagella but not to primary ciliary dyskinesia

Patrick Lorès[1,2,3,†], Charles Coutton[4,5,†], Elma El Khouri[1,2,3,†], Laurence Stouvenel[1,2,3], Maëlle Givelet[1,2,3], Lucie Thomas[6], Baptiste Rode[1,2,3], Alain Schmitt[1,2,3], Bruno Louis[7], Zeinab Sakheli[1,2,3], Marhaba Chaudhry[1,2,3], Angeles Fernandez-Gonzales[8], Alex Mitsialis[8], Denis Dacheux[9,10], Jean-Philippe Wolf[3,11], Jean-François Papon[7,12,13], Gérard Gacon[1,2,3], Estelle Escudier[6,14], Christophe Arnoult[4], Mélanie Bonhivers[10,11], Sergey N. Savinov[15], Serge Amselem[6,14], Pierre F. Ray[4,16,‡], Emmanuel Dulioust[3,11,‡] and Aminata Touré[1,2,3,*,‡]

[1]INSERM U1016, Institut Cochin, Paris 75014, France, [2]Centre National de la Recherche Scientifique UMR8104, Paris 75014, France, [3]Faculté de Médecine, Université Paris Descartes, Sorbonne Paris Cité, Paris 75014, France, [4]Institut for Advanced Biosciences, INSERM U1209, CNRS UMR 5309, Université Grenoble Alpes, 38000 Grenoble, France, [5]CHU Grenoble Alpes, UM de Génétique Chromosomique, Grenoble, France, [6]INSERM UMR S933, Université Pierre et Marie Curie (Paris 6), Paris 75012, France, [7]Equipe 13, INSERM UMR S955, Faculté de Médecine, Université Paris Est, CNRS ERL7240, Créteil 94000, France, [8]Division of Newborn Medicine, Children's Hospital Boston, Boston, MA 02115, USA, [9]Université de Bordeaux, Microbiologie Fondamentale et Pathogénicité, CNRS UMR 5234, Bordeaux, France, [10]Microbiologie Fondamentale et Pathogénicité, Institut Polytechnique de Bordeaux, UMR-CNRS 5234, F-33000 Bordeaux, France, [11]Laboratoire d'Histologie Embryologie–Biologie de la Reproduction, GH Cochin Broca Hôtel Dieu, Assistance Publique-Hôpitaux de Paris, Paris 75014, France, [12]Service d'Oto-Rhino-Laryngologie et de Chirurgie Cervico-Maxillo-Faciale, Hôpital Bicêtre, Assistance Publique – Hôpitaux de Paris, Le Kremlin-Bicêtre 94275, France, [13]Faculté de Médecine, Université Paris-Saclay, Le Kremlin-Bicêtre F-94275, France, [14]Service de Génétique et d'Embryologie Médicales, Hôpital Armand Trousseau, Assistance Publique – Hôpitaux de Paris, Paris 75012, France, [15]Department of Biochemistry and Molecular Biology, University of Massachusetts, Amherst, MA 01003, USA and [16]CHU de Grenoble, UM GI-DPI, Grenoble F-38000, France

[†]These authors contributed equally to this work.
[‡]These authors shared leadership.

Received: December 21, 2017. **Revised:** December 21, 2017. **Accepted:** January 16, 2018

*To whom correspondence should be addressed at: Institut Cochin, INSERMU1016, CNRS UMR8104, Department Development, Reproduction and Cancer, Université Paris Descartes, Paris 75014, France. Tel: +33 144412310; Fax: +33 144412421; Email: aminata.toure@inserm.fr

Abstract

Motile cilia and sperm flagella share an extremely conserved microtubule-based cytoskeleton, called the axoneme, which sustains beating and motility of both organelles. Ultra-structural and/or functional defects of this axoneme are well-known to cause primary ciliary dyskinesia (PCD), a disorder characterized by recurrent respiratory tract infections, chronic otitis media, situs inversus, male infertility and in most severe cases, hydrocephalus. Only recently, mutations in genes encoding axonemal proteins with preferential expression in the testis were identified in isolated male infertility; in those cases, individuals displayed severe asthenozoospermia due to Multiple Morphological Abnormalities of the sperm Flagella (MMAF) but not PCD features. In this study, we performed genetic investigation of two siblings presenting MMAF without any respiratory PCD features, and we report the identification of the c.2018T > G (p.Leu673Pro) transversion in *AK7*, encoding an adenylate kinase, expressed in ciliated tissues and testis. By performing transcript and protein analyses of biological samples from individual carrying the transversion, we demonstrate that this mutation leads to the loss of AK7 protein in sperm cells but not in respiratory ciliated cells, although both cell types carry the mutated transcript and no tissue-specific isoforms were detected. This work therefore, supports the notion that proteins shared by both cilia and sperm flagella may have specific properties and/or function in each organelle, in line with the differences in their mode of assembly and organization. Overall, this work identifies a novel genetic cause of asthenozoospermia due to MMAF and suggests that in humans, more deleterious mutations of AK7 might induce PCD.

Introduction

Cilia are present on almost every cell type in the human body and have emerged as key organelles in many physiological and developmental processes (1,2). In particular motile cilia are present as multiple entities at the surface of several types of epithelial cells, such those in the airways, the oviduct or the brain ventricles, where they cooperatively beat to generate fluid movement. Motile cilia share with the sperm flagella an extremely conserved microtubule-based cytoskeleton, called the axoneme, which sustains beating and motility of both organelles (3,4). This axoneme is composed of a central pair (CP) of microtubules surrounded by nine peripheral microtubules doublets ('9 + 2' pattern) associated with numerous proteins involved in the structure and/or beating coordination (3). The nexin–dynein complexes connect the peripheral doublets to one another and the radial spokes (RSs) connect the peripheral doublets to the CP (5,6). Importantly, the outer- and inner-dynein arms (ODA and IDA), which are multi-protein ATPase complexes, constitute motor elements that associate with the peripheral doublets and drive beating and motility of cilia and flagella (3). In contrast to cilia, sperm flagella contain several peri-axonemal structures delimitating three main compartments in the flagellum: the midpiece, where the axoneme is surrounded by a helical sheath of mitochondria, the principal piece where it is surrounded by the fibrous sheath and the terminal piece devoid of any peri-axonemal structures (7).

Mutations in axonemal proteins, resulting in the loss of IDA, ODA, RS or CP, were initially associated with primary ciliary dyskinesia (PCD, MIM 244400) in human and in mouse (8–10). PCD is a multi-systemic disorder caused by ultra-structural and/or functional defects of motile cilia and flagella (11, 12). The PCD phenotype is mainly characterized by recurrent respiratory tract infections including chronic rhino-sinusitis, otitis and bronchitis leading to bronchiectasis. In approximately 50% of cases, PCD is associated with a situs inversus (i.e. Kartagener syndrome) due to dysfunction of nodal cilia perturbing left-right asymmetry during embryogenesis (13). More rarely, functional impairment of ependymal cilia, in the brain, can cause hydrocephalus in PCD patients (14,15). Importantly, most male individuals with PCD are infertile due to severe sperm motility defects, a condition called asthenozoospermia (12,16).

In recent years, mutations in three genes, *DNAH1*, *CFAP43* and *CFAPA44*, encoding for axonemal proteins mainly present in the sperm, were identified in individuals presenting male infertility but not PCD respiratory features (17–22). Those individuals displayed severe asthenozoospermia due to Multiple Morphological Abnormalities of the sperm Flagella (MMAF syndrome), a phenotype also called 'dysplasia of the fibrous sheath', 'short tails' or 'stump tails', which is characterized by the presence in the ejaculate of a mosaic of spermatozoa with short, irregular, coiled or absent flagella (18). Similar to PCD, the MMAF phenotype was reported to be associated with ultra-structural defects of the flagellar axoneme including the loss of CP, loss of IDA and peripheral doublets disorganization (18,23–26).

In this study, we investigated two infertile siblings showing severe asthenozoospermia and MMAF without any respiratory PCD features, and we report the identification of the c.2018T > G (p.Leu673Pro) missense mutation in *AK7* (MIM: 615364), encoding an adenylate kinase, preferentially expressed in ciliated tissues (27). Adenylate kinases (AKs) are key proteins in maintaining homeostasis of adenine nucleotide pools, by catalysing the reversible transphosphorylation reaction of two molecules of ADP to one molecule each of ATP and AMP (2 ADP $\leftrightarrow$ ATP + AMP). AKs are essential for cell viability as they can salvage energy from ADP in cases of extreme energy utilization and relay energy to compartments that are remote from ATP production sites (27). Assembly and beating of cilia and sperm flagella require a continuous and comprehensive supply of adenosine nucleotides. In agreement, in the mouse, disruption of *AK7* gene resulting in the complete absence of the protein, was shown to induce a PCD phenotype with decreased beat frequency of respiratory cilia, ciliary ultrastructural defects, hydrocephalus and abnormal spermatogenesis (28). In humans, though, reduced amounts of AK7 transcripts and proteins were reported in differentiated nasal epithelial cells and biopsies from PCD individuals (29, 30), so far, no mutations in *AK7* were formally implicated in PCD. Herein, we performed an

exhaustive phenotypical characterization of an individual carrying the c.2018T > G (p.Leu673Pro) transversion and studied the altered transcripts and proteins in semen and cilia samples from the patient. We demonstrate that this missense mutation leads to the absence of AK7 protein in sperm cells but not in respiratory cells, which resulted in primary male infertility without any other PCD features.

Results

Whole-exome sequencing identifies AK7 c.2018T > G (p.Leu673Pro) homozygous mutation in MMAF siblings

In this study, we analysed two siblings, individuals II.1 and II.2, of European descents who both consulted for primary male infertility after unsuccessful natural attempts to conceive children. None of the siblings reported systemic disease or exposure to gonadotoxic factors. Semen analysis of individuals II.1 and II.2 revealed normal sperm count and a moderate decrease in sperm vitality; in contrast, a severe asthenozoospermia with nearly the absence of progressive sperm, was observed (1% and 0%, respectively; normal value ≥ 32%) (Table 1). In addition, very few spermatozoa with normal morphology were present (3 and 5%, respectively; normal value ≥ 23%), and typical MMAF phenotype, defined as the combination of sperm with absent, short, coiled or bent flagella, was diagnosed (Fig. 1A). Ultrastructure analysis of the sperm cells from individual II.1 was performed by transmission electron microscopy (TEM) and showed a severe disorganization of the (9 + 2) axonemal structure; in particular, abnormal midpiece and dysplasia of the fibrous sheath were observed, associated with the lack of CP and disorganization of the peripheral doublets (Fig. 1B).

Both siblings II.1 and II.2 had normal somatic karyotypes (46, XY) and were negative for Y chromosome microdeletions. A notion of consanguinity in the family was mentioned by individual II.1 but the exact degree of consanguinity between the parents was unknown; individuals II.1 and II.2 had also one healthy sister, assessed by general evaluation, who had not yet attempted to have children. We performed whole-exome sequencing (WES) of individual II.1 and based on the family history of consanguinity, we postulated that infertility was likely to be transmitted through recessive inheritance and to result from homozygous mutations. After exclusion of frequent variants and application of technical and biological filters (see 'Materials and Methods' section), a limited list of seven homozygous variants was established (Supplementary Material, Table S1). Six of these homozygous variants were located in genes with very low expression in the testis and *in silico* analysis indicated that they had no deleterious effect (Supplementary Material, Table S1). The last variant was located in *AK7* gene (adenylate kinase 7; GenBank: NM_152327) and corresponded to the homozygous transversion c.2018T > G (p.Leu673Pro), which drew our attention. Indeed, *AK7* was reported in public expression databases and in the literature as strongly expressed in the testis and ciliary tissues (31), and related to cilia and flagella structure and/or functions (28–30). Sanger sequencing was performed and confirmed that the homozygous transversion c.2018T > G was carried by both affected sibling (II.1 and II.2) (Fig. 2A). Analysis of family members indicated that the female sibling (II.3) and both parents (I.1 and I.2) harboured the variant in a heterozygous state (Fig. 2A).

The *AK7* gene is localized on chromosome 14 and contains 18 exons, encoding a predicted 723-amino acid protein (Q96M32) with three principal domains (Fig. 2B). The first domain is close to the N-terminus and contains a WcaG motif, which is a signature of prokaryotic nucleoside diphosphate sugar epimerases, and whose function in AK7 yet remains undetermined. The second domain is the consensus ADK domain, which is composed of a large central CORE region containing the p-loop domain (phosphate donor binding glycine rich region) flanked with the NMP domain (AMP-binding domain) and the LID domain (ATP-binding domain) (32). In addition, and in contrast to all other known paralogs (AK1–6; AK8–9), the AK7 protein harbours a DPY30 domain, located at the C-terminus part of the protein, which is a motif involved in protein oligomerization and docking found in many proteins including axonemal proteins (33,34). The transversion c.2018T > G is located in exon 17 of *AK7* (Genbank NM_152327), and replaces the leucine residue at position 673 by a proline residue (p.Leu673Pro), in an extended helix of a coiled-coil (CC) domain, preceding the DPY30 domain (Fig. 2B); this leucine residue, as well as the flanking amino acids L672 and E674, were found to be highly conserved during evolution (Fig. 2C). *In silico* analysis was performed and the p.Leu673Pro variant was unequivocally considered as damaging by prediction software (see 'Materials and Methods' section). Lastly, the analysis of 123 136 exomes and 15 496 genomes, aggregated in the gnomAD database (http://gnomad.broadinstitute.org/), indicated that the c.2018T > G (p.Leu673Pro) variant, referenced as rs116298211, was present at a prevalence of 1.49e-3 (413/277106 alleles) in the general population; such low prevalence being consistent with negative selection of the mutation and a recessive transmission. Taking into account (i) the established ciliary expression pattern of *AK7*, (ii) the above *in silico* data indicating the pathogenicity of the c.2018T > G (p.Leu673Pro) variant identified in *AK7*, (iii) the familial segregation and (iv) the absence of other variants in genes significantly expressed in testis and/or related to cilia/flagellum, we focused on *AK7*, which appeared as the best candidate to explain the primary male infertility observed in the two siblings.

Sperm from *Ak7*$^{-/-}$ mouse present ultrastructural defects of the flagella similar to those observed in sperm from MMAF individuals

The PCD phenotype observed in *Ak7*$^{-/-}$ mice due to ubiquitous absence of the protein, was exhaustively characterized and reported by Fernandez-Gonzalez et al.; in addition, a preliminary analysis of the reproductive organs indicated that testes and epididymes of *Ak7*$^{-/-}$ mice were devoid of sperm cells (28). In order to provide additional argument supporting the pathogenicity of the p.Leu673Pro mutation in the two MMAF siblings, we performed new analyses on *Ak7*$^{-/-}$ mice. We delineated the sperm ultra-structural phenotype of *Ak7*$^{-/-}$ mice, by performing TEM analysis on testicular and epididymal sperm. Analyses of *Ak7*$^{-/-}$ testes revealed the absence of flagellum structures, compared with testes from control littermates. In *Ak7*$^{-/-}$ testes, nearly all sperm heads were attached to cytoplasmic mass and these heads were not prolonged by flagellar structures such as mitochondrial sheath, fibrous sheath and axoneme (Fig. 3). In *Ak7*$^{-/-}$ epididymes, very few sperm structures could be observed. Importantly, the rare transversal sections of *Ak7*$^{-/-}$ null sperm flagellum that could be observed showed an absence of the CP, which is a feature found in sperm from individual II.1 (Fig. 3). These data indicate that although the phenotype of *Ak7*$^{-/-}$ mice is more severe, the structural defects of the axoneme observed in *Ak7*$^{-/-}$ null sperm are similar to those we found in sperm from MMAF individuals carrying the

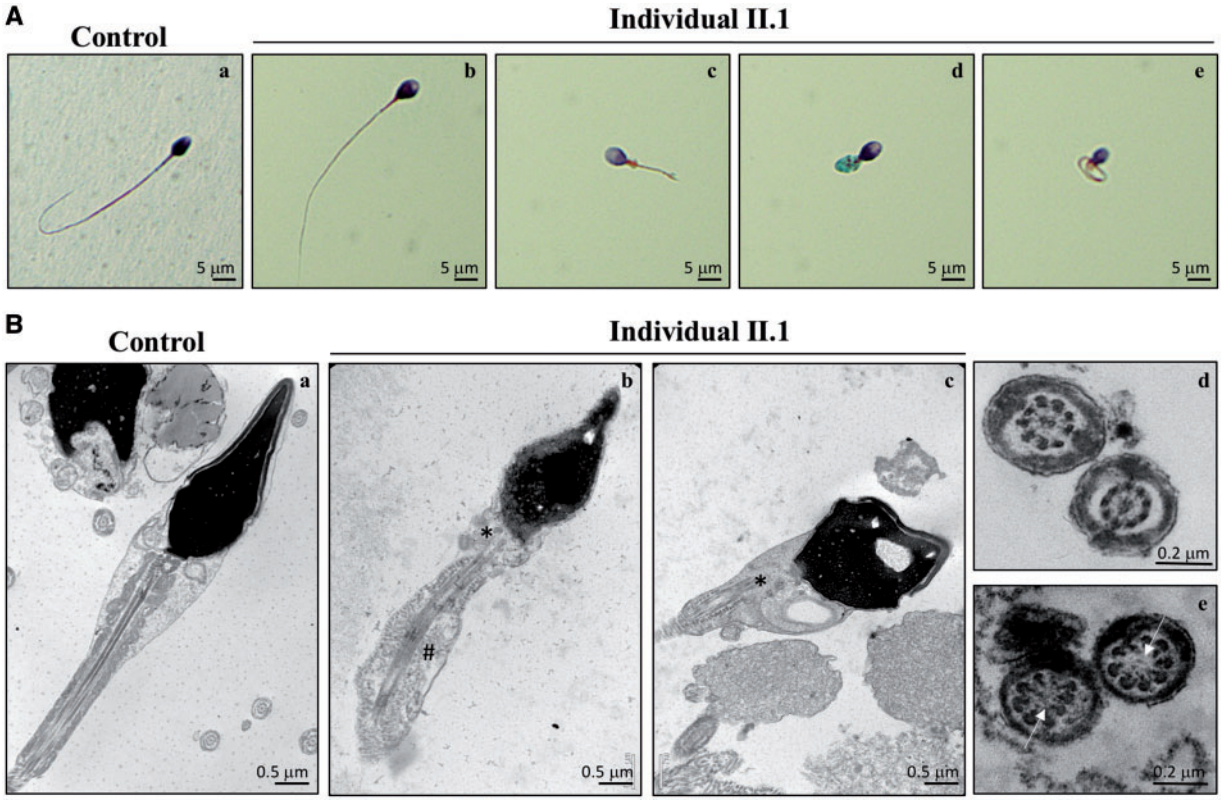

Figure 1. Morphology and ultrastructure of spermatozoa from individual II.1. (**A**) In contrast to control individual (a), spermatozoa with normal morphology were only occasionally observed in sperm preparation from individual II.1 (b). The majority of the sperm (97%) in individual II.1 had short flagella and additional features of MMAF such as thick, absent and coiled flagella (c–e). Scale bars represent 5µm. (**B**) Electron microscopy analysis of semen sample from individual II.1 indicated, as previously reported for MMAF individuals, abnormal and incomplete mitochondrial sheath (*; b, c), dysplasia of the fibrous sheath (#; b), and disorganization of the axonemal structure with lack of the central pair of microtubules (white arrow; e). Control (a, d); individual II.1 (b, c, e). Scale bars represent 0.5 µm (a–c) and 0.2 µm (d, e).

Table 1. Semen parameters of individuals II.1 and II.2 compared with normal values. Values are expressed in percent, unless specified otherwise

	Age (years)	Sperm volume (ml)	Total sperm count (10^6/ejaculate)	Total Motility (PR + NP)	Progressive Motility (PR)	Vitality	Morphology (typical forms)
Reference limits[a]	n.a	>1.5	39	>40	>32	>58	>23
Individual II.1	39	4.2	52.5	13	1	48	3
Individual II.2	38	5	150	3	0	–	5

[a]Reference limits according to the World Health Organization (WHO) standards (77) and the distribution range of morphologically normal spermatozoa observed in fertile individuals (78).

n.a: not applicable. PR: Progressive motility, which corresponds to rapid and slow progressive spermatozoa (formerly grades a and b, respectively). NP: Non-progressive motility, which corresponds to static spermatozoa (i.e. motile but non-progressive spermatozoa; formerly grade c).

homozygous c.2018T > G (p.Leu673Pro) transversion, therefore supporting the pathogenicity of this mutation.

AK7 protein is detected in human spermatozoa and locates to the sperm flagellum

Expression of human and mouse *AK7* gene in the testis and ciliated tissues was reported in public expression databases (EMBL-EBI Expression Atlas; Riken Famtom5 Project) and in the literature (28,31) but no information was available regarding AK7 protein distribution in spermatozoa. We thus, first analysed AK7 protein on human sperm cells from control individuals by means of western blot and immunofluorescence microscopy. AK7 protein was detected, at the predicted molecular weight of 83 kDa, in sperm protein extracts from control individuals (Fig. 4A, left panel). In addition, AK7 immunostaining was detected along the full length of the sperm flagellum and co-localized with α-Tubulin (Fig. 4A, right panel), consistent with the pattern of an axonemal component.

AK7 protein is absent in sperm cells but present in airway epithelial cells from individual II.1 carrying the c.2018T > G (p.Leu673Pro) transversion

In order to assess *in vivo* the impact of the *c.2018T > G* (p.Leu673Pro) variant, we sought to analyse AK7 protein distribution in sperm and airway epithelial cells (AEC) from both individuals carrying the transversion; however, only individual II.1

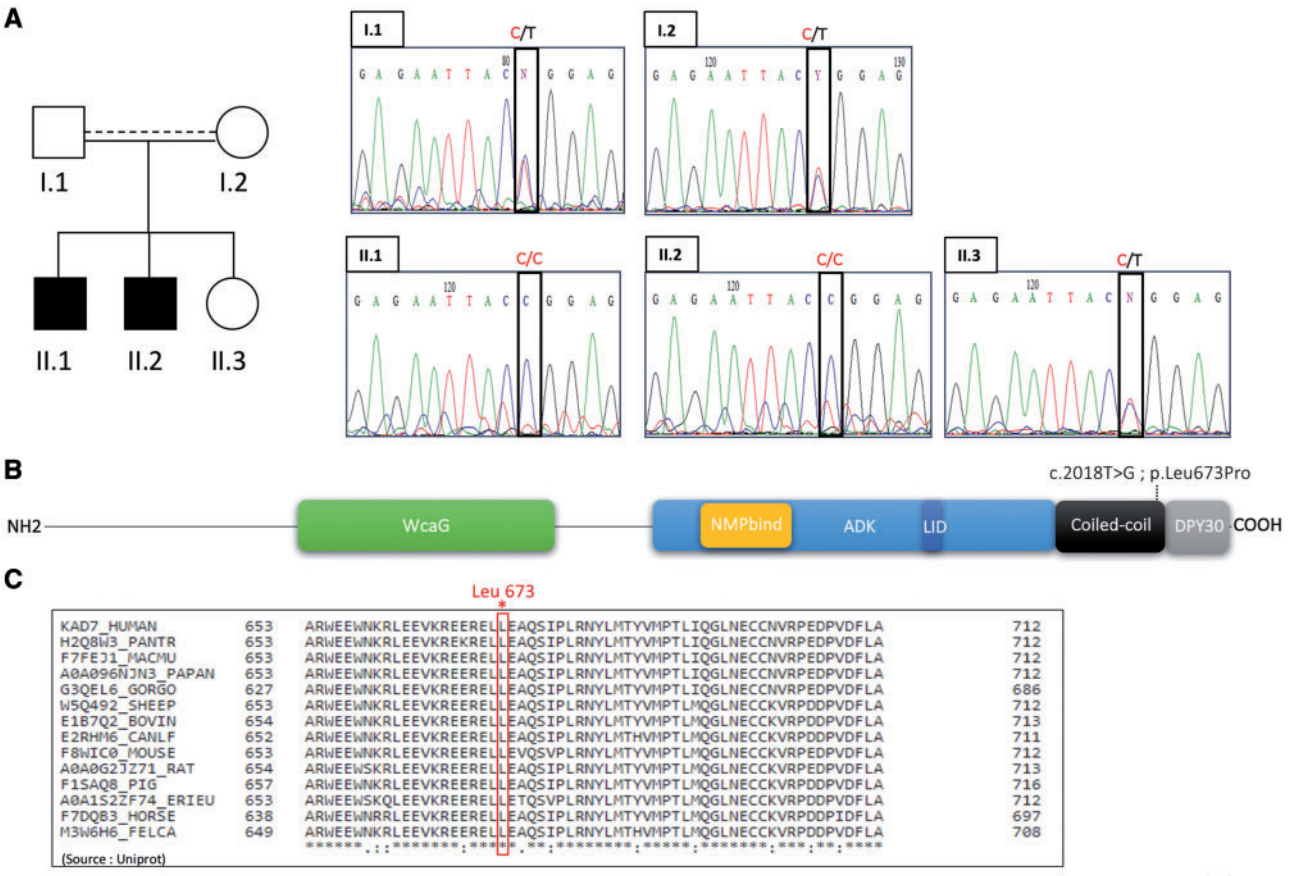

Figure 2. Genetic tree of the studied family and location of the mutation in AK7 protein. (**A**) Pedigrees of individual II.1 and II.2 with MMAF phenotype in whom WES was performed and identified the homozygous c.2018T > G (p.Leu673Pro) transversion. The dashed line indicates consanguinity between parents (I.1 and I.2). The presence of the identified variation c.2018T > G; p.Leu673Pro (NM_152327) was verified by Sanger sequencing of *AK7* exon 17. All members from the family, including the second infertile sibling (II.2), were sequenced for the mutation. Electrophoregrams of *AK7* exon 17 showing the mutated sequence are presented. The two infertile siblings (II.1 and II.2) carried a homozygous missense mutation (p.Leu673Pro) in *AK7* exon 17 whereas their sister (II.3) and parents (I.1 and I.2) harbour the mutation in a heterozygous state. (**B**) Schematic representation of the functional domains of AK7 (SMART: http://smart.embl-heidelberg.de/). The green box indicates the N-terminus domain containing a WcaG motif; the blue box indicates the ADK domain comprising the ATP-binding domain (LID, dark blue box) and the AMP-binding domain (NMP, orange box) and the grey box represents the DPY30 domain located in the C-terminal part. The mutation c.2018T > G; p.Leu673Pro (NM_152327) changes Leucine at position 673 into a Proline. The Leu673Pro mutation is located in a helix of the coiled-coil domain (CC, dark box) domain in close proximity to the DPY30 domain of AK7 (COIL program, http://www.ch.embnet.org/software/COILS_form.html). (**C**) Partial sequence alignment of AK7 proteins shows the evolutionary conservation of the Leu673 residue (*), which is mutated in individuals II.1 and II.2 (http://www.uniprot.org/blast/).

agreed to further participate to the research program. Western blot analysis on sperm protein extracts showed significant AK7 signal for the control but no signal for individual II.1, whereas DNAI1, a component of the ODAs, was equally detected in both individuals (Fig. 4B, left panel). To confirm these results, we performed immunodetection assays. Here again, we observed that the AK7 protein was not detected on sperm cells from individual II.1, even when these cells succeeded in assembling a flagellum, which was visualized by α-tubulin staining (Fig. 4C). In order to rule out the possibility that AK7 protein is non-specifically eliminated from the sperm due to abnormal biogenesis of the flagellum, we investigated AK7 protein in sperm protein extracts from four MMAF individuals (MMAF P1–4) who do not carry any mutation in AK7 coding sequence. These subjects were described previously in (22): one carried mutations in the *CFAP43* gene and was identified as P_{43}–9 (MMAF P1), one had a homozygous *DNAH1* mutation and was identified as P_{DNA}-5 (MMAF P2) and two had no identified mutations (MMAF P3 and P4). Data from exome sequencing showed that in these four subjects, all AK7 exons were well covered (coverage > 10 as established using the igv software) but did not evidence any deleterious variant in AK7. We found that the AK7 protein was present in sperm flagella from the four MMAF individuals we tested (Supplementary Material, Fig S1). Therefore, we conclude that the absence of AK7 protein in sperm cells from individual II.1 is not a constant feature of MMAF individuals, and is very likely induced by the *c.2018T > G* (p.Leu673Pro) transversion. We next evaluated the impact of the mutation in respiratory ciliated cells from individual II.1 by performing Western blot experiments on AECs, collected after nasal brushing. Surprisingly, in contrast to what was observed in the sperm cells, AK7 protein was detected in AECs from individual II.1, as well as in AECs from control individual (Fig. 4B, right panel).

Individual II.1 carrying the c.2018T > G (p.Leu673Pro) variant, displays normal nasal cilia structure and function and has no respiratory PCD features

We further investigated individual II.1 for established respiratory features of PCD and performed structural and functional

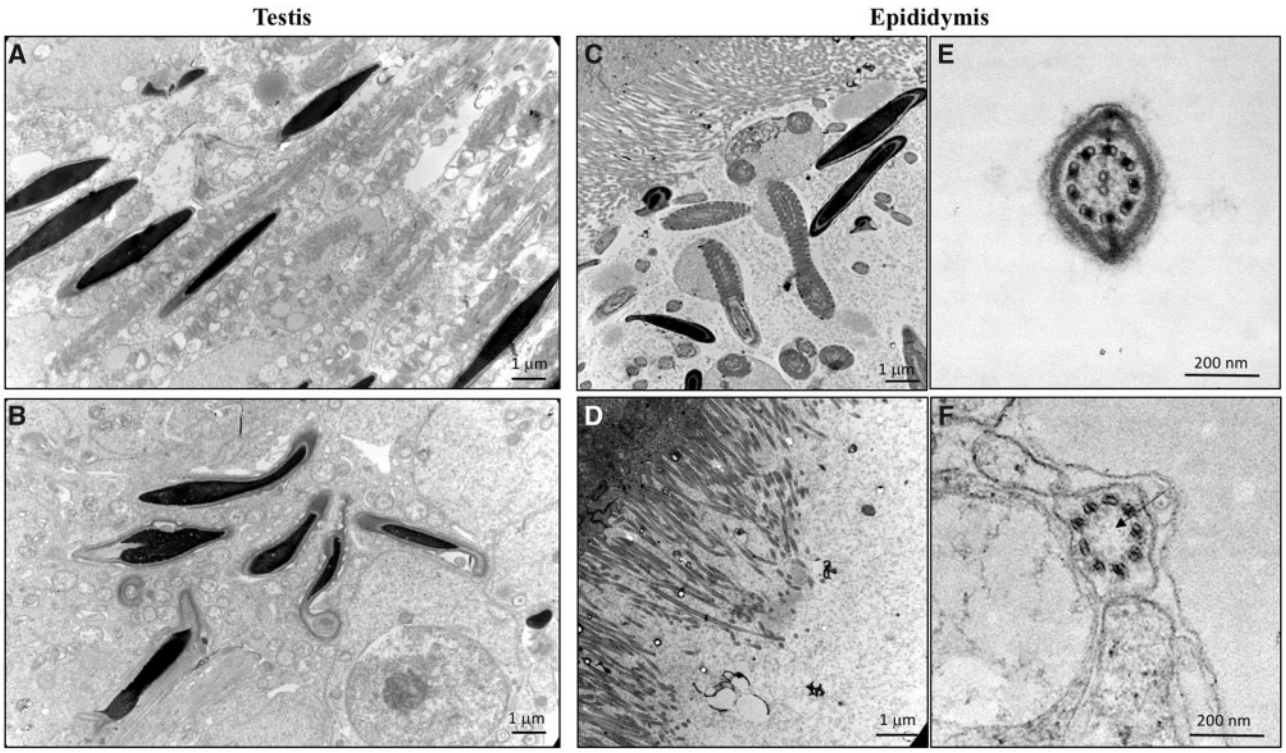

Figure 3. Ultrastructure analyses of sperm cells from $Ak7^{-/-}$ mice testes and epididymes by TEM. In contrast to testes from control litter mates (**A**), analysis of testes from $Ak7^{-/-}$ mice indicated the presence of sperm head without elongated flagella (**B**). In addition, analysis of epididymes from $Ak7^{-/-}$ mice indicated the absence of sperm structures; in contrast to epididymes from control litter mates (**C**), almost no sperm heads, nor transversal/longitudinal sections of flagellum are observed (**D**). The rare transversal sections of $Ak7^{-/-}$ flagella, which were observed in the epididymes were abnormal (**F**), compared with wild type sperm (**E**) and do not present the central pair of microtubules (black arrow). Control (A, C, E); $AK7^{-/-}$ (B, D, F). Scale bars represent 1µm (A–D) and 200nm (E, F).

characterization of respiratory cilia. Clinical interrogation indicated that individual II.1 presented mild rhinosinusitis episodes during childhood, but did not exhibit classical PCD symptoms, which associate bronchitis, bronchiectasis and otitis media with effusion. CT-scan of the ear, nose and throat (ENT) as well as audiogram, were normal; and at the day of the ENT evaluation, the global score for rhinologic and otologic symptoms was null. TEM analysis of the respiratory cilia showed normal structure of the ciliary axoneme; the peripheral doublets of microtubules and the central pair were constantly observed in all section analysed (Fig. 5A). In addition, nasal nitric oxide (NO) levels of individual II.1 were normal (2406 ppb), based on reference values (35), and high-speed video microscopy (HSV) indicated normal ciliary beating frequency (CBF) and pattern (Fig. 5B). Thus, consistently with the persistence of AK7 protein in AEC protein samples, individual II.1 does not present any respiratory features of PCD but isolated male infertility.

Analysis of AK7 transcript isoforms in spermatozoa and AEC of control individuals and individual II.1

In order to determine the impact of the c.2018T > G transversion on AK7 transcripts, we performed RT-PCR experiments on sperm cells and AEC from control individual and individual II.1. We first examined transcript sequences available in databases and found three coding transcripts described in Ensembl (http://www.ensembl.org/index.html): the main transcript AK7–201 (ENST00000267584.8) of 3300bp and 18 exons, which encodes the predicted protein of 83kDa (723 amino acids), and two short transcripts: transcript AK7–204, only containing exon 1 and 2 (ENST00000555570.1), and transcript AK7–203 containing exons 16, 17 and a modified exon 18 (ENST00000554706.1). These two short transcripts only encode for proteins of 107 and 152 amino-acids, respectively, and could not have produced the full-size protein corresponding to the 83kD band, which we observed on Western blot analyses; we therefore focused on AK7 main transcript, which we further investigated in biological samples from individual II.1.

In order to assess if AK7 main transcript (AK7–201; ENST00000267584.8) is present in AEC and sperm cells from individual II.1, we performed RT-PCR using primers F4 and R4, located upstream from the mutation, in exons 15 and 16, respectively (Fig. 6A). Amplification of AK7 transcript was obtained for both patient and control, in the two tested tissues and no difference of pattern was observed (Fig. 6B); in parallel, amplification of the ubiquitous housekeeping gene *HPRT*, confirmed equal amount and quality of the amplified cDNAs (Fig. 6B). Next, although we detected the AK7 protein at the expected size in AEC, we tested the possibility that it could have been translated specifically in this tissue from an alternative transcript devoid of exon 17, where the mutation is located. For this purpose, we performed RT-PCR experiments using primers F4 and R3, located in exons 15 and 18, respectively (Fig. 6A). A unique band of the expected size of 537 bp was observed in both sperm and AEC samples from individual II.1 (Fig. 6C). Similar results were obtained when using primers F2 and R2 located in exon 16 and the 3'UTR region, respectively (data not shown). We therefore exclude the possibility of an alternative transcript of AK7 devoid of exon 17, with specific expression in AEC. Finally, though unlikely, it is possible that the identified

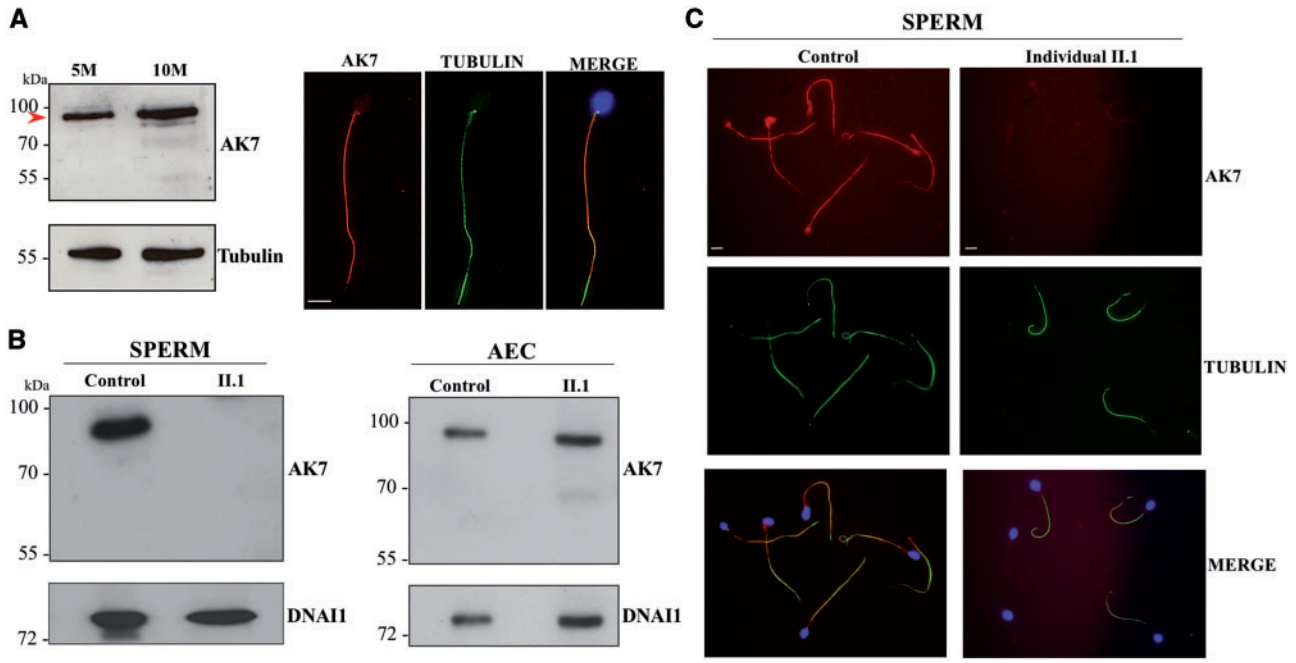

Figure 4. AK7 protein detection and localization in human sperm cells from control individual and in biological samples from individual II.1 carrying the c.2018T > G; p.Leu673Pro transversion. (**A**) Left panel: AK7 protein was detected by Western blot analysis on protein extracts from human spermatozoa (5 and 10 million), at a molecular weight compatible with the predicted size of 83 kDa. Right panel: Immunofluorescence staining of human spermatozoa from healthy fertile controls revealed AK7 co-localization with α-Tubulin along the flagellum. Scale bars represent 5μm. (**B**) Left panel: AK7 protein was not detected in sperm protein extract from individual II.1, in contrast to healthy and fertile individual; whereas DNAI1 was equally detected in sperm form individual II.1 and control ($N = 4$). Right panel: AK7 protein was detected in AEC protein extract from both healthy individual and individual II.1 carrying the c.2018T > G; p.Leu673Pro transversion ($N = 3$). (**C**) When performing immunofluorescence assay, the AK7 protein (red) was not detected in sperm from individual II.1, in contrast to control sperm. DNA was counterstained with DAPI in the merge picture. Scale bars represent 5μm.

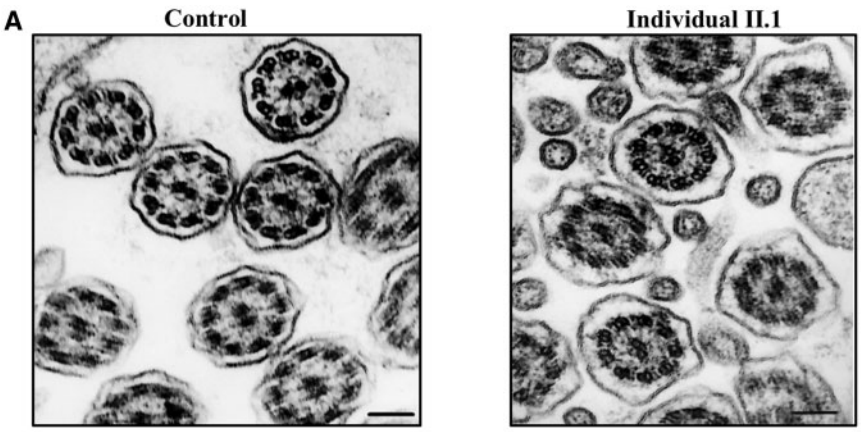

B

	Beating cilia (%)	CBF (Hz)	Angle (°)	Distance travelled per sec (μm)
Controls (mean ± SD)	91±13	8.9±2	71.6±6.6	66.7±14.2
Individual II.1	100	11.1±3.3	58±17	63.8±29.1

Figure 5. Ultrastructural and functional analyses of nasal respiratory ciliated cells from individual II.1 carrying the homozygous mutation c.2018T > G in AK7. (**A**) Electron micrographs of cross-sections of AEC from a control individual and from individual II.1. For each individual, several axonemal sections are shown with a well-organized configuration (9 + 2), the presence of dynein arms and the central pair. Black scale bars represent 0.1μm. (**B**) High speed video microscopy parameters of respiratory ciliated cells from individual II.1 and controls. Normal ciliary beating frequency and pattern were observed for individual II.A. CBF: ciliary beating frequency (in Hertz); SD: standard deviation.

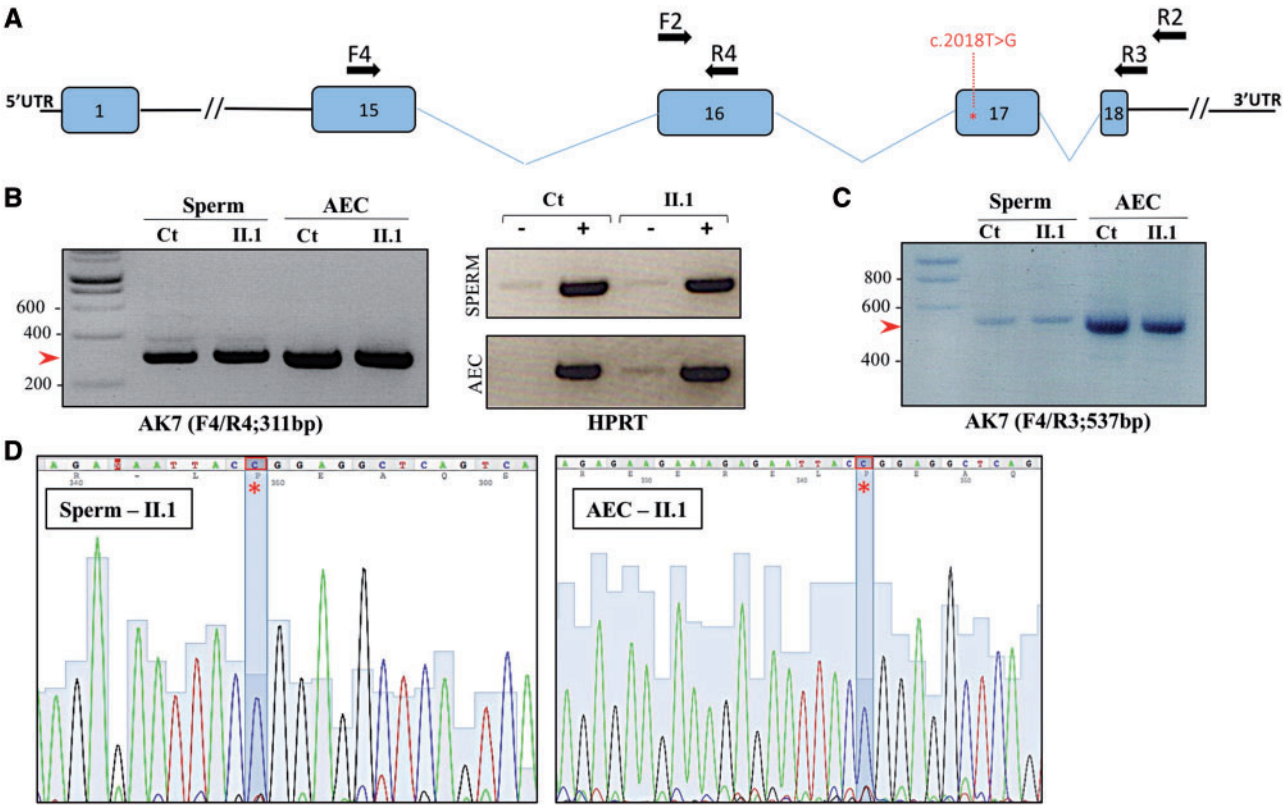

Figure 6. Analysis of AK7 transcripts in sperm and AEC from control individual and individual II.1 carrying the c.2018T > G; p.Leu673Pro transversion. **(A)** Scheme of AK7 exons and introns structure surrounding the exon 17 where is located the c.2018T > G; p.Leu673Pro transversion. The set of primers used for RT-PCR are positioned above the corresponding transcript sequence. **(B)** Left panel: RT-PCR analysis of AK7 transcript (ENST00000267584.8) using primers F4 and R4 revealed no differences between sperm from individual II.1 and sperm from control individual. Similar result is obtained for AEC. Right panel: Quality and quantity control of cDNA amplification. HPRT amplification products obtained from RNA incubated with (+) and without (−) reverse transcriptase (RT) are presented for both control individual and individual II.1. **(C)** RT-PCR analysis of AK7 transcript (ENST00000267584.8) using primers F4 and R3 shows the absence of lower bands transcripts devoid of exon 17, even when higher amounts of AEC transcripts are loaded. **(D)** Sequencing of the RT-PCR fragment amplified from AEC and sperm from individual II.1, using primers F4 and R3. Electrophoregrams showed that all cDNAs amplified from individual II.1 carried the c.2018T > G variant, in both sperm cells and AEC.

mutation is present in mosaic in the patient; we therefore sequenced the RT-PCR fragment amplified with primers F4 and R3, in AEC and sperm from individual II.1. Sequence analysis showed that all cDNAs amplified from individual II.1 carried the c.2018T > G variant (Fig. 6D). We therefore demonstrated that in subject II.1 and controls, only one transcript is present in both sperm cells and AECs and that in subject II.1, the mutation is present in the transcript detected in both cell types. This indicates that i.) in both tissues, the c.2018T > G variant does not affect AK7 transcription and ii.) transcript degradation or alternative splicing cannot explain the loss of the AK7 protein in sperm.

In silico modelling of AK7 C-terminus (613–723) region

The c.2018T > G (p.Leu673Pro) transversion replaces the leucine residue at position 673 by a proline residue, in a linker region (aa 613–678) located between the ADK domain and the DPY30 domain, predicted with a coiled-coil structure. Using a range of molecular modelling and bioinformatic tools, we intended to generate a model of the c-terminal region of AK7 (613–723) and to test potential impact of the p.Leu673Pro variation on the structure.

No gap-free homology templates for the spacer fragment (aa 613–678) could be identified in the PDB database, but we could establish the preference of this region for a helical conformation on the basis of (i) amino acid composition (84.3 and 98.4% of helix-forming and non-helix-breaking residues, respectively) (36), (ii) primary sequence ($i/i+3$ and $i/i+4$ distribution of lipophilic residues through amphipathic fragments), (iii) overlapping reassembly of gap-free homologous helical templates (pdb's: 102D [605–615], 3BHP [616–620], 2MVM [621–631], 5AJ3 [632–659], 4OYD [660–676], and 4RTA [677–723]), and iv) prediction by COILS program (37), which assigns contiguous helicity to the 613/614–677/678 region, with coiled-coil propensity.

Next, we used the Dpy30C-Bre2$_{DBM}$ crystal structure available in structure databases, Pdb 4RT4, as a template for homology modelling of AK7 C-terminus (613–723). In this structure, the Bre2$_{DBM}$ peptide was inserted in a groove and interacted with Dpy30 mainly through hydrophobic interactions (Fig. 7A). Importantly Zhang et al. reported that the Bre2$_{DBM}$ peptide simultaneously interacts with two Dpy30 dimers, forming a tetrameric structure (Fig. 7A) (38,39). We generated the theoretical dimeric structure of AK7, which retained 48% of residues of the 4RT4 template at the homo-dimer interface (within 4Å), by superimposing the monomer models onto the template structure, and next refining the structure by protonation/tautomerization states reassignment and minimization (Fig. 7B). The resulting complex featured a largely hydrophobic groove furnished with a tetrad of exposed arginine residues capable of accommodating a helical amphipathic (lipophilic and acidic) ligand(s) (34) (Fig. 7B). In addition, the C-terminal dimer of AK7

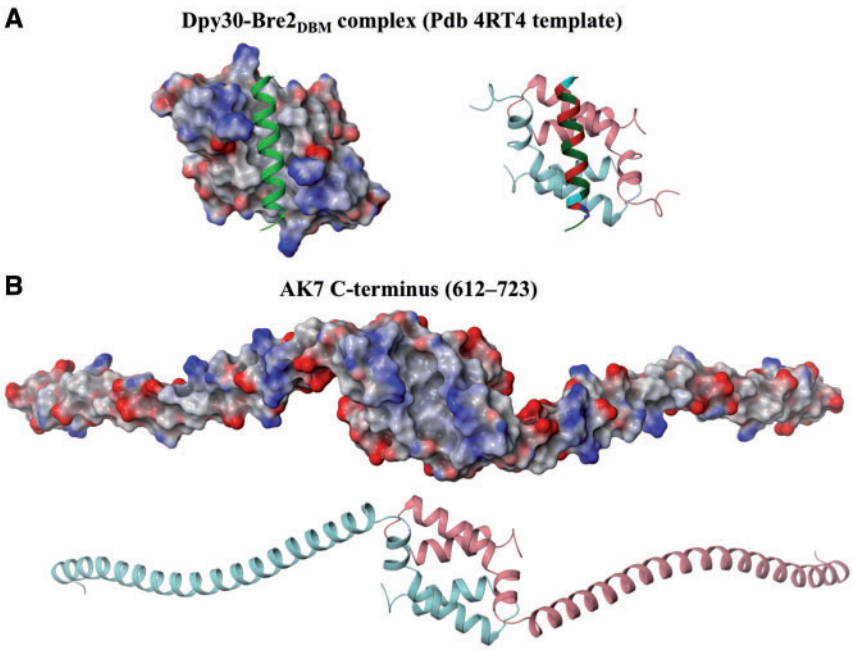

Figure 7. In silico modelling of AK7 C-terminus (613–723), established by homology using the crystal structure of the Dpy30-Bre2$_{DBM}$ complex as a template. (**A**) Crystal structure of the Dpy30-Bre2$_{DBM}$ complex (pdb: 4RT4), which contains a dimer of Dpy30 and one copy of Bre2$_{DBM}$ peptid$_e$. On the left, the Dpy30 dimer is shown as electronic potential surface and the Bre2 helix ligand is shown as a green ribbon, which is inserted in a groove and interacts with Dpy30 through mainly hydrophobic interactions. On the right, the Dpy30 dimer is shown as ribbons and the Bre2 helix is colored by residue properties (dark green: hydrophobic, red: acidic, blue: basic and cyan: polar neutral). Schrodinger's Small-Molecule Drug Discovery suite of programs (v. 2016–1, Schrodinger, LLC): https://www.schrodinger.com/) (**B**) Homology model established for the C-terminus of AK7 (612–723). On the top, the AK7 C-terminus dimer is shown as electronic potential surface; similar to the Dpy30 structure, the AK7 model contains a largely hydrophobic groove furnished with a tetrad of exposed arginine residues capable of accommodating a helical amphipathic. On the bottom, AK7 dimeric structure is represented as ribbons. Schrodinger's Small-Molecule Drug Discovery suite of programs (v. 2016–1, Schrodinger, LLC): https://www.schrodinger.com/).

continues to expose most of the lipophilic residues from the helical linker, including Leu672/Leu673 tandem, as well as a pair of conserved tryptophan residues (Trp655 and Trp658). This is notable, because while tryptophan is the most enriched residue at protein–protein interfaces (40), it is rather uncommon for coiled-coil regions (41), which suggested further capacity for intra- or inter-dimer protein–protein contact. In consistence with this, we could establish a homology model of AK7 tetrameric structure, in a manner reminiscent of the Dpy30 tetrameric complex (39) (Supplementary Material, Fig. S2A and B). Interestingly, the helical linker of AK7 (aa 613–678) exhibits high, but non-uniform level of conservation with sequenced orthologues (Supplementary Material, Fig. S3A and B). The high level of conservation of the C-terminal half of the linker, including residue 673, along with the predicted coiled-coil propensity of this region, supports its participation in oligomerization of the dimeric AK7. Altogether, our data indicate that the C-terminal region of AK7 is associated with oligomerization properties, as described for others proteins harbouring a DPY30 domain (33,34), and that the structure of this region contains a hydrophobic groove, which may interact with helical amphipathic (lipophilic and acidic) ligand(s).

The c.2018T > G (p.Leu673Pro) variation does not impact AK7 protein amounts *in vitro* but impacts AK7 protein structure

The above transcript and protein analyses indicated that the lack of AK7 protein observed in the sperm cells of individual II.1 is likely to result from defects occurring at the protein level and specifically in this cell type. Therefore, we first tested if the c.2018T > G (p.Leu673Pro) transversion impacts protein production and/or degradation. For this purpose, we transfected Hela cells with eukaryotic expression vectors containing the wild-type, FLAG-AK7_WT, or the variant protein, FLAG-AK7_Leu673Pro. Immunoblot analyses of protein lysates after 24 and 48 h of transfection indicated similar amounts of WT_AK7 and mutant AK7_Leu673Pro proteins (Supplementary Material, Fig. S4A). To confirm these results and test for a potential specific effect in the germline, we performed transient transfection in CHO cells and in the mouse spermatogonial cell line GC1, respectively. Similar results were obtained in CHO cells (data not shown) and GC1 cells (Supplementary Material, Fig. S4A). These results suggest that *in vitro*, the presence of the Leu673Pro variant does not alter protein synthesis and does not induce protein degradation.

The p.Leu673Pro variation replaces the hydrophobic leucine residue by a similarly hydrophobic but cyclic proline residue, which, lacking the NH backbone for hydrogen bonding, is recognized as the most effective amino acid in disrupting regular secondary structure elements, such as α-helices and β-sheets and is known to favour turn and loop arrangements (42). Since the Leucine 673 is located within a predicted helix acting as a linker between the ADK and DPY-30 domains, we expect that the p.Leu673Pro variation will misdirect the extended helix and perturb oligomerization interface. To test these hypotheses, we used the COILS program (http://www.ch.embnet.org/software/COILS_form.html), and compared the scores of helix propensity obtained for the wild type and the mutated proteins. The results obtained clearly indicated that the p.Leu673Pro mutation affects the coiled-coil propensity of AK7 linker region; the prediction

score obtained for the linker sequence following residue 673 was 0.904 for the wild-type sequence (Leu673) but dropped to 0.560 and 0.454 for the mutated sequence (Pro673) (Supplementary Material, Fig. S4B). Therefore, we concluded that the p.Leu673Pro variation perturbs the stability of the helix and destabilizes the coiled-coil region upstream of the DPY30 domain, which, in turn, may compromise the assembly and/or anchorage of axonemal protein complexes involving AK7 in the sperm.

The c.2018T > G (p.Leu673Pro) variation impacts AKAP4 protein distribution in sperm from individual II.A

In order to provide arguments supporting the above hypothesis, we further characterized sperm from individual II.1 by performing a series of immunostaining with antibodies targeting proteins which locate to various axonemal and peri-axonemal structures of the sperm flagellum. We observed that in sperm from individual II.1 that extended a flagellum visualized by α-Tubulin staining, the staining for DNAI2, DNAL1I, SPAG6, RSPH1 and DNAH1 was generally similar to what we observed in sperm from control individual (although DNALI1 staining was remarkably weaker in some sperm from individual II.1). These data suggested that the protein complexes, which constitute ODA, IDA, CP and RS heads were not primarily affected by the AK7 mutation (Supplementary Material, Figs S5–S7). However, when analysing AKAP4, one of the main proteins of the fibrous sheath, which is also known to interact with DPY30 motif containing proteins (43), we observed an abnormal and heterogeneous staining of the sperm flagella in comparison with control sperm (Fig. 8). While some sperm from individual II.1 displayed an AKAP4 staining similar to control cells, remarkably, in nearly half of the sperm cells, the AKAP4 staining was faint, absent and occasionally, discontinuous (Fig. 8; Supplementary Material, Fig. S8), whereas α-tubulin staining was well detected. Importantly, such heterogeneous staining pattern for AKAP4 protein distribution was not previously observed in sperm from MMAF patients who do not carry any mutation in AK7 (22). To confirm that this abnormal AKAP4 staining pattern was specific to the sperm from individual II.1, we analysed sperm from MMAF Patient P4, in which we previously detected normal amount of AK7 protein by western blot (Supplementary Material, Fig. S1); we observed that in sperm from patient P4, the AKAP4 staining was similar to staining observed in controls sperm cells (Supplementary Material, Fig. S8). Therefore, we concluded that, *in vivo*, the c.2018T > G (p.Leu673Pro) variant identified in AK7 is associated with the lack of AK7 protein together with abnormal distribution of AKAP4 protein in the sperm flagellum.

Discussion

In the present study, we have analysed two siblings presenting with male primary infertility and MMAF phenotype. Genetic investigations of the family led to the identification of the homozygous c.2018T > G (p.Leu673Pro) mutation in *AK7* carried by both affected siblings, and transmitted through recessive inheritance.

While in the mouse, the ubiquitous loss of AK7 protein was associated with PCD (28), so far, in humans, no mutation in AK7 were formally implicated in PCD. Interestingly, no PCD features were observed in individual carrying the c.2018T > G (p.Leu673Pro) transversion, even after exhaustive clinical and functional investigations of cilia function. This is consistent with the fact that normal AK7 gene expression and protein production were observed in AECs from this individual. Conversely, we showed that the p.Leu673Pro mutation is associated with a total absence of AK7 protein in mature spermatozoa from individual II.1, which was not observed in MMAF individuals with different genetic aetiology. Importantly, in AECs we did not evidence alternative transcripts that could explain the detection of the protein in these cells; in addition, both AECs and sperm cells from individual II.1 were shown to harbour only the mutated transcript. These findings indicated that some functional properties of the AK7 protein itself were differently impacted in sperm cells and in AECs by the p.Leu673Pro mutation. *In vitro* and *in silico* experiments confirmed that the p.Leu673Pro mutation does not hamper protein levels *in vitro* but is likely to impact the structure of the coil-coiled domain preceding the DPY30 domain, which constitutes an interaction and oligomerization domain, as observed in other proteins. Altogether, these results indicate that the absence of AK7 in the sperm cells from individual II.1 is not due to defective gene expression, defective protein production but is likely to be induced by structural defects impacting interaction of the protein with axonemal partners and/or anchoring within the axoneme in the sperm cells.

The sperm flagellum is assembled during the last step of spermatogenesis called spermiogenesis. This process is associated with a dramatic reduction of the cell size and elimination in residual bodies of the excess of cytoplasm which contains components that are not needed for further sperm function (44–46). Improper structure and interaction of the mutated AK7 protein with axonemal partner(s), may therefore lead to the exclusion of the AK7 mutated protein from the axoneme during flagellum assembly and elimination in the residual bodies within the testis. Importantly, we showed that AK7 protein elimination is not a constant feature of MMAF individuals as the AK7 protein was detected in sperm protein extracts from MMAF individuals who do not carry any AK7 mutation. Alternatively, or in addition, although we did not observe abnormal protein levels *in vitro*, upon transient transfection of eukaryotic vectors expressing the mutated AK7 protein in different cell types, one cannot exclude that *in vivo*, the mutated AK7 protein may be degraded by a sperm-specific protein quality control/proteasome machinery (47–49). Supporting this hypothesis, several testis and/or sperm-specific ubiquitination enzymes from the ubiquitin/proteasome machinery have been described in rodents and humans (50–53). Overall, our data indicate that the p. Leu673Pro mutation differentially affects AK7 protein in sperm cells and AEC, leading to isolated primary male infertility without respiratory features of PCD. Hence, while in sperm cells, the p.Leu673Pro mutation causes the absence of AK7 protein, in AECs the p.Leu673Pro mutation does not impact AK7 protein amount and moreover the presence of AK7 protein harbouring the p. Leu673Pro mutation does not interfere with ciliary structure and function. The absence of ciliary phenotype suggests that the mutated AK7 protein is still able to fulfil its functions in cilia and/or that the DPY30 domain, which is presumably impacted by the p.Leu673Pro mutation, is only essential for axoneme assembly in the sperm and not in AEC.

The importance of AK activity in sperm is emphasized when considering structural limitations of this cell, such as the compartmentalization of mitochondria, restraining generation of the ATP by oxidative phosphorylation to the midpiece, and the length of the flagellum, which can reach 100 μm in some species. Accordingly, numerous AK isoforms were identified as components of axonemal and peri-axonemal structures in mouse sperm flagella (*AK1*, *AK2*, *AK7* and *AK8*) (54,55) and in

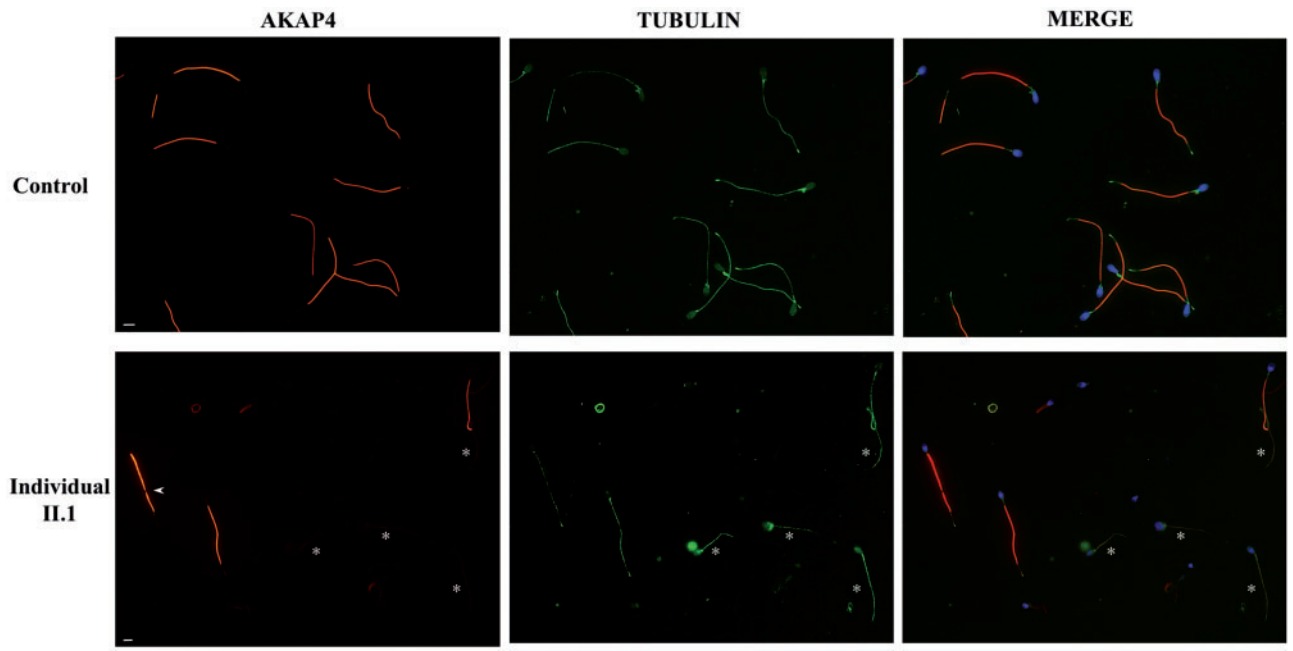

Figure 8. Representative immunofluorescence detection of AKAP4 protein in human sperm cells from control individual and individual II.1 carrying the c.2018T > G; p.Leu673Pro transversion. In sperm from control individual, AKAP4 protein (red) was detected in the principal piece of the flagellum while α-Tubulin staining (green) covered all the flagellum length. In sperm from individual II.1, AKAP4 staining (red) was heterogeneous as most sperm cells displayed weak or no signal (*), while α-Tubulin staining (green) was detected. In a few sperm a discontinuous staining was also observed (arrow). DNA was counterstained with DAPI in the merge picture. Scale bars represent 5 μm.

flagellated protists such as *T. brucei (ADK1 and ADKB, ADKE)* (56) and *Chlamydomonas* (57). Phylogenetic analysis indicates that AK7 orthologs are found in mammals, reptiles, birds, fishes, amphibians and in some ciliated protozoan such as Tetrahymena and *T. brucei* but not in Chlamydomonas (http://www.ensembl.org; http://www.genecards.org). Interestingly, among all existing adenylate kinases, AK7 is the only member, which contains a DPY30 domain, located at the carboxy-terminal extremity of the protein. We can speculate that the DPY30 domain in AK7 protein is essential for specific targeting of AK activity close to axonemal components, such as the dyneins molecular complexes, which are involved in flagella beating and require constant energy supply.

The DPY30 domain presents homology in sequence and structure with the RIIa domain of the cAMP-dependent protein kinase A (PKA), which allows binding to the A-kinase anchoring proteins (AKAPs) (43). Similar to the RIIa domain (33), the DPY30 domain is found in over hundreds of proteins (43,58), implicated in diverse critical processes such as membrane trafficking (59), histone methylation (60), stem cell differentiation (61) and flagellar beating (62). Importantly, in *Chlamydomonas*, while no strict ortholog of AK7 is identified (Ensembl: http://www.ensembl.org), the radial spoke protein RSP2, which harbours a DPY30 domain, is required for correct assembly of the spoke heads and normal axonemal structure; and mutation of RSP2 leads to flagella paralysis in *Chlamydomonas* (33). Using a range of bioinformatic tools, we performed molecular modelling of AK7 C-terminal region, which includes the extended helix where the p.Leu673Pro mutation locates, and the DPY30 domain. We provide several arguments indicating that the C-terminal region of AK7 is involved in homo- and/or hetero-oligomerization of AK7, in a manner reminiscent of the dimeric RSP2 protein. Overall, our data indicate that the p.Leu673Pro variation is predicted to destabilize the coiled-coil region upstream of the DPY30 domain, which may compromise assembly, anchorage and/or function of the axonemal complexes involving AK7 in the sperm.

To date, no information is available concerning AK7 partners in the sperm flagellum. When considering the DPY30 domain, *AKAP3* (MIM: 604689) and *AKAP4* (MIM: 300185), which encode for the most abundant structural proteins of the sperm fibrous sheath (63) constitute potential candidates. In line with this hypothesis, we observed an abnormal distribution of AKAP4 protein in sperm from individual II.1, which was not observed in sperm from MMAF individuals carrying mutations in other genes. In addition, partial deletion of *AKAP3* and *AKAP4* were previously found in an infertile patient presenting a MMAF-like phenotype (64), and invalidation of Akap4 in the mouse (65) also presented a similar phenotype. Other potential AK7 partners are suggested by the observations of a tight association of adenylate kinases with axonemal components of the flagellum, such as dynein arms (57,66,67). In *Tetrahymena*, proteome and interactome analyses identified a molecular complex involving the flagellar associated protein FAP251, AK7 and other DPY30 motif-containing proteins (68) together with DNAH1 (formerly named DHC7; MIM: 60332), an inner dynein arm heavy chain directly linked to the RS complex (18,69). Importantly, DNAH1 mutations were identified in MMAF individuals with severe axonemal defects, including loss of the CP, as observed in individual II.1 carrying the p.Leu673Pro mutation in AK7 (18). Altogether, the above data suggest that AK7 play a role in axonemal multiprotein complexes, involving dynein and components of the RS; thus, similar to mutations in genes encoding components of the RS (70–74), mutations in AK7 are expected to induce defects of the CP. In the future, proteomic studies of axonemal components in mammalian cells may provide a comprehensive and comparative map of AK7 interactome in the axoneme of sperm cells versus cilia.

In total, our work demonstrates the importance of AK7 in the structure and function of the sperm axoneme. Importantly, we show that although the axoneme is a highly conserved central cytoskeletal structure shared by both the sperm flagellum and motile cilia (3,75), the p.Leu673Pro mutation identified in AK7 is only deleterious for the sperm cells and does not impact respiratory ciliated cells; thus preventing the manifestations of PCD symptoms. These observations support the notion that proteins shared by both cilia and sperm flagella, may have specific properties and/or function in each organelle, in line with the differences in their mode of assembly and organization (7,76). The missense mutation we identified is unique by inducing a deleterious effect in sperm cells and not in respiratory ciliated cells; we therefore anticipate that only a small subset of AK7 mutations will produce the MMAF phenotype described here, and that truncating mutations may induce PCD, as illustrated by the mouse model. Overall, our work identifies a novel genetic cause of asthenozoospermia due to MMAF and indicates that in humans, more deleterious mutations in AK7 resulting in the global absence of AK7 protein, are likely to induce PCD with CP defects, a subset of PCD for which few genes have been implicated so far (8,9).

Materials and Methods

Biological samples

Informed consent was obtained from all the individuals participating in the study according to the local protocols and the principles of the Declaration of Helsinki. The study was conducted with the approval of the Comité de Protection des Personnes CPP Ile de France III (approval Nos. CPP02748 and CPP07729).

DNA was extracted from blood or saliva samples from the two siblings and their first-degree relatives. Semen samples were obtained by masturbation after a period of three to five days of sexual abstinence. Semen samples were incubated at 37°C for 30 min for liquefaction; ejaculate volume and pH, sperm concentration, vitality, morphology and motility were evaluated according to World Health Organization (WHO) guidelines (77). Sperm vitality was assessed by eosin staining, and sperm morphology was analysed on Schorr stained semen smears according to David's classification (78). All control individuals from the study displayed normal values of semen parameters compared with the WHO guidelines. Airway epithelial cells were obtained by brushing or biopsy of the middle part of the inferior turbinate and used for immunofluorescence assay and ciliary investigations. Ciliary investigations were performed when individual was free of airway tract infection or respiratory exacerbation for at least 6 weeks.

WES and bioinformatics analysis

Genomic DNA from saliva was isolated using Oragen DNA extraction kit (DNAgenotech®, Ottawa, Canada). Coding regions and intron/exon boundaries were enriched using the 'all Exon V5 kit' (Agilent Technologies, Wokingham, UK). DNA sequencing was undertaken at the Genoscope, Evry, France, on the HiSeq 2000 from Illumina®. Sequence reads were aligned to the reference genome (hg19) using MAGIC (79). MAGIC produces quality-adjusted variant and reference read counts on each strand at every covered position in the genome. Duplicate reads and reads that mapped to multiple locations in the genome were excluded from further analysis. Positions with sequence coverage below 10 on either the forward or reverse strand were marked as low confidence, and positions with coverage below 10 on both strands were excluded. Single nucleotide variations (SNV) and small insertions/deletions (indels) were identified and quality-filtered using in-house scripts. Briefly, for each variant, independent calls were made on each strand, and only positions where both calls agree are retained. The most promising candidate variants were identified using an in-house bioinformatics pipeline, as follows. Variants with a minor allele frequency greater than 5% in the NHLBI ESP6500 [Exome Variant Server, NHLBI GO Exome Sequencing Project (ESP), Seattle, WA] or in 1000 Genomes Project phase 1 datasets (80), or greater than 1% in ExAC (PMID 27535533), were discarded. All variants present in homozygous state in this database were excluded. We used Variant Effect Predictor [VEP version 81(PMID 27268795)] to predict the impact of the selected variants.

Sanger sequencing

The selected mutation in *AK7* gene was validated by Sanger sequencing using primers 5'-GGT GAC CAT TTC TAG CAG TG-3' and 5'-CGC CAC ACC CAA ACT CAA AT-3'. Sequencing was carried out on ABI 3130XL (Applied Biosystems) and analyses were performed using SeqScape software (Applied Biosystems).

Transmission electron microscopy

Human sperm cells (10 millions) or mouse testes and epididymes were fixed by incubation in 0.1 M phosphate buffer pH 7 supplemented with 3% glutaraldehyde (Grade I; Sigma-Aldrich Co.) for 2 h at room temperature. The samples were washed twice in PBS and resuspended in 0.2 M sodium cacodylate buffer. The samples were then post-fixed by incubation with 1% osmium tetroxide (Electron Microscopy Sciences, Hatfield, UK), after which they were dehydrated by immersion in a graded series of alcohol solutions and embedded in Epon resin (Polysciences Inc., Warrington, USA). Semi-thin sections were cut and stained with toluidine blue-Azur II. Ultra-thin sections (90 nm) were cut with a Reichert Ultracut S ultramicrotome (Reichert-Jung AG, Wien, Austria) and were then stained with uranyl acetate and lead citrate. Sections were analysed with a JEOL 1011 microscope and digital images were acquired with a Gatan Erlangshen CCD camera and Digital Micrograph software.

Immunofluorescence assays

10 μl of semen sample were spread onto a Superfrost Plus slide (Menzel Glasbearbeitungswerk, GmbH & Co. KG, Braunschweig, Germany). Sperm was fixed by incubation with PBS/4% paraformaldehyde for 10 min. The slides were treated with 0.2% Triton in PBS for permeabilization and then blocked by incubation in 1% BSA for 1 h. They were then incubated with primary antibodies for 2 h at room temperature and then secondary antibodies for 1 h at room temperature. The slides were mounted in Vectashield medium (Vector Laboratories, Burlingame, USA) supplemented with 0.5 mg/ml DAPI. Slides were analysed with a Zeiss Axiophot epifluorescence microscope. Digital images were acquired with a cooled charge-coupled device (CCD) camera (Hamamatsu Co. Japan), under identical instrument settings, with MetaMorph® software (Molecular Devices, Inc. USA). Details of antibodies and dilutions used for immunofluorescence assays are provided in Supplementary Material, Table S3.

Protein extraction and immunoblotting

For immunoblotting experiments, cells were washed with PBS and lysed in cold buffer A [50 mM Tris-HCl, pH 8, 150 mM NaCl, 10 mM $MgCl_2$, 0.5% NP40 (Sigma), protease Inhibitor cocktail (Roche)]. Samples were incubated for 30 min at 4°C and then centrifuged for 20 min at 13 000 g and 4°C. Protein quantification was carried out by using the *BC Assay* reagent (Interchim). After denaturation (5 min at 95°C) in Laemmli sample buffer, equal amounts of protein were subjected to SDS-PAGE [14% acrylamide/bisacrylamide (40% 37.5: 1)] and transferred onto nitrocellulose membranes. The membranes were blocked in 5% milk in PBS-Tween 0.1%, and immunoblot analysis was performed using the indicated primary antibodies.

The primary antibodies used were polyclonal rabbit anti-AK7 antibodies (Sigma HPA003543; 1: 50 dilution), monoclonal mouse anti-α-tubulin antibodies (Sigma T9026; 1: 2500 dilution), polyclonal rabbit anti-DNAI1 antibodies (Sigma HPA021649; 1: 250 dilution).

The secondary antibodies used were rabbit polyclonal anti-mouse Ig coupled to Horse Radish Peroxydase (HRP) (Dako; 1: 1000 dilution), swine polyclonal antirabbit Ig coupled to HRP (Dako; 1: 500 dilution), goat anti-rabbit Alexa-fluor 568 (Invitrogen, Molecular Probes; 1: 500 dilution) and anti-mouse Alexa-fluor 488 (Invitrogen, Molecular Probes; 1: 500 dilution).

RT-PCR experiments

800–1000 ng of total RNA from spermatozoa or AEC were extracted using NucleoSpin RNA kit (Macherey-Nagel, Düren, German) and subjected to reverse transcription with High-Capacity cDNA Reverse Transcription Kit [Applied Biosystems, Thermo Fisher Scientific, following the manufacturer's instructions.

PCR reactions were performed with GoTaq® DNA Polymerase (Promega, Madison, WI, USA) using specific primers to amplify AK7 transcript (ENST00000267584.8) and HPRT.

Sequences of primers used and expected product sizes are summarized in Supplementary Material, Table S4.

Cilia structure and function

The ciliary ultrastructure was analysed by TEM on nasal biopsy immediately immersed in glutaraldehyde as previously described (81). Results are expressed as the percentage of abnormal cilia among the number of analysed cilia (at least 50 per patient). The ciliary beating was analysed by high speed videomicroscopy (HSV) as previously described (82). Epithelial cells were immediately immersed in B1 BSA medium (CCD®, Paris, France) and examined within 3 h, during a maximum of 20 min, at room temperature, with an optic microscope (Axiovert 200, Carl Zeiss®, Le Pecq, France). Using an oil immersion x100 objective, we recorded a minimum of 10 video captures of 10 different ciliated edges viewed from the side, with a digital high-speed camera (A741, PixeLink®, Ottawa, Canada), at 358 frames per second with a definition of 256 × 192 pixels (1800 frames, ~5 seconds per video). Isolated ciliated cells were not considered. We performed 10 beating analyses from 10 different ciliated edges, including the percentage of beating cilia, the ciliary beat frequency (CBF) and a qualitative evaluation of the beat pattern.

In silico protein modelling and sequence alignment

All computational procedures were carried out using Schrodinger's Small-Molecule Drug Discovery suite of programs (v. 2016–1, Schrodinger, LLC): Maestro, BioLuminate, Epic, Prime and Desmond (https://www.schrodinger.com/). For homology modeling, we used Prime's Homology Modeling workflow and for splicing homology fragments together, we used BioLuminate's Protein Splicing tool. The energy optimized all-atom model was generated via a protonation state assignment (Epic) and constrained minimization (Prime) sequence within Maestro's Protein Preparation Wizard (Schrodinger LLC). For protein–protein docking, we used BioLuminate's Protein–Protein Docking tool. The final structures were rendered using Maestro's Surface and Ribbons tools.

Sequence alignment was performed using the blastp suite of BLAST (Basic Local Alignment Search Tool) for non-redundant protein sequences and the results were filtered for orthologous sequences down to 85% identity for the full sequence (https://blast.ncbi.nlm.nih.gov/Blast.cgi).

The sequences were processed and rendered using Multiple Sequence Viewer tool within Maestro.

Cell culture and transfection

Cells [Chinese Hamster Ovary (CHO-K1), Germ Cell 1 (GC1) and Henrietta Lacks (HeLa)] were maintained at 37°C in a 5% CO_2 atmosphere, in DMEM GlutaMAX medium (Invitrogen) supplemented with 10% fetal bovine serum, 100U/ml Penicillin, 100 μg/ml Streptomycin and 0.25 μg/ml Fungizone. The cells were transiently transfected using the *Jet Pei (Polyplus)* reagent according to the manufacturer's instructions.

Supplementary Material

Supplementary Material is available at *HMG* online.

Acknowledgements

We thank all individuals and their family for their cooperation, as well as all referring physicians. We thank all the technicians from the *Service de Biologie de la Reproduction* (Hôpital Cochin, Paris) for routine semen sample evaluation. We thank the Cellular Imaging Facility of Institut Cochin (INSERM U1016, CNRS UMR8104, Université Paris Descartes), in particular, Jean-Marc Massé and Azzedine Yacia for electron microscopy procedures.

Conflict of Interest statement. None declared.

Funding

This work was supported by the Institut National de la Santé et de la Recherche Médicale (INSERM); the Centre National de la Recherche Scientifique (CNRS); the Université Paris Descartes, the Université Pierre et Marie Curie; and the Agence Nationale de la Recherche [MUCOFERTIL 12-BSV1–0011 to AT; MASFLAGELLA 14-CE15 to PR, AT and MB].

Web Resources

The URLs for data presented herein are as follows:
1000 genomes: www.internationalgenome.org/
BLAST: https://blast.ncbi.nlm.nih.gov/Blast.cgi

COILS: http://www.ch.embnet.org/software/COILS_form.html
ExAC browser: exac.broadinstitute.org/
Exome Variant Server: evs.gs.washington.edu/
gnomAD database: (http://gnomad.broadinstitute.org/
OMIM: http://www.omim.org
Polyphen-2: genetics.bwh.harvard.edu/pph2
RefSeq: http://www.ncbi.nlm.nih.gov/RefSeq
SIFT: sift.jcvi.org
Schrodinger's Small-Molecule Drug Discovery suite of programs (v. 2016–1, Schrodinger, LLC): https://www.schrodinger.com/
SMART: http://smart.embl-heidelberg.de/
UNIPROT: http://www.uniprot.org

References

1. Bisgrove, B.W. and Yost, H.J. (2006) The roles of cilia in developmental disorders and disease. *Development*, **133**, 4131–4143.
2. Mitchison, H.M. and Valente, E.M. (2017) Motile and non-motile cilia in human pathology: from function to phenotypes. *J. Pathol.*, **241**, 294–309.
3. Satir, P. and Christensen, S.T. (2007) Overview of structure and function of mammalian cilia. *Ann. Rev. Physiol.*, **69**, 377–400.
4. Ishikawa, H. and Marshall, W.F. (2011) Ciliogenesis: building the cell's antenna. *Nat. Rev. Mol. Cell Biol.*, **12**, 222–234.
5. Curry, A.M. and Rosenbaum, J.L. (1993) Flagellar radial spoke: a model molecular genetic system for studying organelle assembly. *Cell Motil. Cytoskeleton*, **24**, 224–232.
6. Smith, E.F. and Yang, P. (2004) The radial spokes and central apparatus: mechano-chemical transducers that regulate flagellar motility. *Cell Motil. Cytoskeleton*, **57**, 8–17.
7. Holstein, A.F.C. and Roosen Runge, E.C. (1981) *Atlas of Human Spermatogenesis*. Grosse Verlag, Berlin.
8. Horani, A., Ferkol, T.W., Dutcher, S.K. and Brody, S.L. (2016) Genetics and biology of primary ciliary dyskinesia. *Paediatr. Respir. Rev.*, **18**, 18–24.
9. Kurkowiak, M., Ziętkiewicz, E. and Witt, M. (2015) Recent advances in primary ciliary dyskinesia genetics. *J. Med. Genet.*, **52**, 1–9.
10. Lee, S., Fan, C.Y., Younger, J.M., Ren, H. and Cyr, D.M. (2002) Identification of essential residues in the type II Hsp40 Sis1 that function in polypeptide binding. *J. Biol. Chem.*, **277**, 21675–21682.
11. Afzelius, B.A. (1985) The immotile-cilia syndrome: a microtubule-associated defect. *CRC Crit. Rev. Biochem.*, **19**, 63–87.
12. Knowles, M.R., Zariwala, M. and Leigh, M. (2016) Primary ciliary dyskinesia. *Clin. Chest Med.*, **37**, 449–461.
13. Leigh, M.W., Pittman, J.E., Carson, J.L., Ferkol, T.W., Dell, S.D., Davis, S.D., Knowles, M.R. and Zariwala, M.A. (2009) Clinical and genetic aspects of primary ciliary dyskinesia/Kartagener syndrome. *Genet. Med.*, **11**, 473–487.
14. Ibanez-Tallon, I., Heintz, N. and Omran, H. (2003) To beat or not to beat: roles of cilia in development and disease. *Hum. Mol. Genet.*, **12 Spec No 1**, R27–R35.
15. Kosaki, K., Ikeda, K., Miyakoshi, K., Ueno, M., Kosaki, R., Takahashi, D., Tanaka, M., Torikata, C., Yoshimura, Y. and Takahashi, T. (2004) Absent inner dynein arms in a fetus with familial hydrocephalus-situs abnormality. *Am. J. Med. Genet. A*, **129A**, 308–311.
16. Homma, K., Miller, K.K., Anderson, C.T., Sengupta, S., Du, G.G., Aguinaga, S., Cheatham, M., Dallos, P. and Zheng, J. (2010) Interaction between CFTR and prestin (SLC26A5). *Biochim. Et Biophys. Acta*, **1798**, 1029–1040.
17. Amiri-Yekta, A., Coutton, C., Kherraf, Z.-E., Karaouzène, T., Le Tanno, P., Sanati, M.H., Sabbaghian, M., Almadani, N., Sadighi Gilani, M.A., Hosseini, S.H. *et al.* (2016) Whole-exome sequencing of familial cases of multiple morphological abnormalities of the sperm flagella (MMAF) reveals new DNAH1 mutations. *Hum. Reprod.*, **31**, 2872–2880.
18. Ben Khelifa, M., Coutton, C., Zouari, R., Karaouzène, T., Rendu, J., Bidart, M., Yassine, S., Pierre, V., Delaroche, J., Hennebicq, S. *et al.* (2014) Mutations in DNAH1, which encodes an inner arm heavy chain dynein, lead to male infertility from multiple morphological abnormalities of the sperm flagella. *Am. J. Hum. Genet.*, **94**, 95–104.
19. Sha, Y., Yang, X., Mei, L., Ji, Z., Wang, X., Ding, L., Li, P. and Yang, S. (2017) DNAH1 gene mutations and their potential association with dysplasia of the sperm fibrous sheath and infertility in the Han Chinese population. *Fertil. Steril.*, **107**, 1312–1318 e1312.
20. Tang, S., Wang, X., Li, W., Yang, X., Li, Z., Liu, W., Li, C., Zhu, Z., Wang, L., Wang, J. *et al.* (2017) Biallelic mutations in CFAP43 and CFAP44 cause male infertility with multiple morphological abnormalities of the sperm flagella. *Am. J. Hum. Genet.*, **100**, 854–864.
21. Wang, X., Jin, H., Han, F., Cui, Y., Chen, J., Yang, C., Zhu, P., Wang, W., Jiao, G., Wang, W. *et al.* (2017) Homozygous DNAH1 frameshift mutation causes multiple morphological anomalies of the sperm flagella in Chinese. *Clin. Genet.*, **91**, 313–321.
22. Coutton, C., Vargas, A., Amiri-Yekta, A., Kherraf, Z.-E., Fourati Ben Mustapha, S., Le Tanno, P., Wambergue-Legrand, C., Karaouzène, T., Martinez, G., Crouzy, S. *et al.* (2018) Mutations in CFAP43 and CFAP44 cause male infertility and flagellum defects in Trypanosoma and human. *Nat Commun*, in press, doi: 10.1038/s41467-41017-02792-41467.
23. Chemes, H.E., Brugo, S., Zanchetti, F., Carrere, C. and Lavieri, J.C. (1987) Dysplasia of the fibrous sheath: an ultrastructural defect of human spermatozoa associated with sperm immotility and primary sterility. *Fertil. Steril.*, **48**, 664–669.
24. Escalier, D. (2006) Arrest of flagellum morphogenesis with fibrous sheath immaturity of human spermatozoa. *Andrologia*, **38**, 54–60.
25. Escalier, D. (2003) New insights into the assembly of the periaxonemal structures in mammalian spermatozoa. *Biol. Reprod.*, **69**, 373–378.
26. David, G., Feneux, D., Serres, C., Escalier, D. and Jouannet, P. (1993) [A new entity of sperm pathology: peri-axonemal flagellar dyskinesia]. *Bull. Acad. Natl Med.*, **177**, 263–271. discussion 272-265.
27. Dzeja, P. and Terzic, A. (2009) Adenylate kinase and AMP signaling networks: metabolic monitoring, signal communication and body energy sensing. *Int. J. Mol. Sci.*, **10**, 1729–1772.
28. Fernandez-Gonzalez, A., Kourembanas, S., Wyatt, T.A. and Mitsialis, S.A. (2009) Mutation of murine adenylate kinase 7 underlies a primary ciliary dyskinesia phenotype. *Am. J. Respir. Cell Mol. Biol.*, **40**, 305–313.
29. Milara, J., Armengot, M., Mata, M., Morcillo, E.J. and Cortijo, J. (2010) Role of adenylate kinase type 7 expression on cilia motility: possible link in primary ciliary dyskinesia. *Am. J. Rhinol. Allergy*, **24**, 181–185.
30. Mata, M., Lluch-Estelles, J., Armengot, M., Sarrion, I., Carda, C. and Cortijo, J. (2012) New adenylate kinase 7 (AK7) mutation in primary ciliary dyskinesia. *Am. J. Rhinol. Allergy*, **26**, 260–264.

31. Ivliev, A.E., 't Hoen, P.A.C., van Roon-Mom, W.M.C., Peters, D.J.M., Sergeeva, M.G. and Dias-Neto, E. (2012) Exploring the transcriptome of ciliated cells using in silico dissection of human tissues. *PLoS One*, **7**, e35618.
32. Panayiotou, C., Solaroli, N. and Karlsson, A. (2014) The many isoforms of human adenylate kinases. *Int. J. Biochem. Cell Biol.*, **49**, 75–83.
33. Gopal, R., Foster, K.W. and Yang, P. (2012) The DPY-30 domain and its flanking sequence mediate the assembly and modulation of flagellar radial spoke complexes. *Mol. Cell Biol.*, **32**, 4012–4024.
34. Sivadas, P., Dienes, J.M., St Maurice, M., Meek, W.D. and Yang, P. (2012) A flagellar A-kinase anchoring protein with two amphipathic helices forms a structural scaffold in the radial spoke complex. *J. Cell Biol.*, **199**, 639–651.
35. Collins, S.A., Gove, K., Walker, W. and Lucas, J.S. (2014) Nasal nitric oxide screening for primary ciliary dyskinesia: systematic review and meta-analysis. *Eur. Respir. J.*, **44**, 1589–1599.
36. Chou, P.Y. and Fasman, G.D. (1978) Empirical predictions of protein conformation. *Annu. Rev. Biochem.*, **47**, 251–276.
37. Lupas, A., Van Dyke, M. and Stock, J. (1991) Predicting coiled coils from protein sequences. *Science*, **252**, 1162–1164.
38. South, P.F., Fingerman, I.M., Mersman, D.P., Du, H.N. and Briggs, S.D. (2010) A conserved interaction between the SDI domain of Bre2 and the Dpy-30 domain of Sdc1 is required for histone methylation and gene expression. *J. Biol. Chem.*, **285**, 595–607.
39. Zhang, H., Li, M., Gao, Y., Jia, C., Pan, X., Cao, P., Zhao, X., Zhang, J. and Chang, W. (2015) Structural implications of Dpy30 oligomerization for MLL/SET1 COMPASS H3K4 trimethylation. *Protein Cell*, **6**, 147–151.
40. Mohamed, R., Degac, J., Helms, V. and Sticht, H. (2015) Composition of overlapping protein-protein and protein-ligand interfaces. *PLoS One*, **10**, e0140965.
41. Surkont, J. and Pereira-Leal, J.B. (2015) Evolutionary patterns in coiled-coils. *Genome Biol. Evol.*, **7**, 545–556.
42. Krieger, F., Moglich, A. and Kiefhaber, T. (2005) Effect of proline and glycine residues on dynamics and barriers of loop formation in polypeptide chains. *J. Am. Chem. Soc.*, **127**, 3346–3352.
43. Welch, E.J., Jones, B.W. and Scott, J.D. (2010) Networking with AKAPs: context-dependent regulation of anchored enzymes. *Mol. Interv.*, **10**, 86–97.
44. Machaca, K., DeFelice, L.J. and L'Hernault, S.W. (1996) A novel chloride channel localizes to Caenorhabditis elegans spermatids and chloride channel blockers induce spermatid differentiation. *Dev. Biol.*, **176**, 1–16.
45. L'Hernault, S.W. (2006) Spermatogenesis. *WormBook*, 1–14.
46. Huang, J., Wang, H., Chen, Y., Wang, X. and Zhang, H. (2012) Residual body removal during spermatogenesis in C. elegans requires genes that mediate cell corpse clearance. *Development*, **139**, 4613–4622.
47. Zimmerman, S. and Sutovsky, P. (2009) The sperm proteasome during sperm capacitation and fertilization. *J. Reprod. Immunol.*, **83**, 19–25.
48. Sutovsky, P. (2011) Sperm proteasome and fertilization. *Reprod. Suppl.*, **142**, 1–14.
49. Morales, P., Kong, M., Pizarro, E. and Pasten, C. (2003) Participation of the sperm proteasome in human fertilization. *Hum. Reprod.*, **18**, 1010–1017.
50. Mochida, K., Tres, L.L. and Kierszenbaum, A.L. (2000) Structural features of the 26S proteasome complex isolated from rat testis and sperm tail. *Mol. Reprod. Dev.*, **57**, 176–184.
51. Nishito, Y., Hasegawa, M., Inohara, N. and Nunez, G. (2006) MEX is a testis-specific E3 ubiquitin ligase that promotes death receptor-induced apoptosis. *Biochem. J.*, **396**, 411–417.
52. Mitchell, M.J., Woods, D.R., Tucker, P.K., Opp, J.S. and Bishop, C.E. (1991) Homology of a candidate spermatogenic gene from the mouse Y chromosome to the ubiquitin-activating enzyme E1. *Nature*, **354**, 483–486.
53. Liu, Y.Q., Bai, G., Zhang, H., Su, D., Tao, D.C., Yang, Y., Ma, Y.X. and Zhang, S.Z. (2010) Human RING finger protein ZNF645 is a novel testis-specific E3 ubiquitin ligase. *Asian J. Androl.*, **12**, 658–666.
54. Cao, W., Haig-Ladewig, L., Gerton, G.L. and Moss, S.B. (2006) Adenylate kinases 1 and 2 are part of the accessory structures in the mouse sperm flagellum. *Biol. Reprod.*, **75**, 492–500.
55. Vadnais, M.L., Cao, W., Aghajanian, H.K., Haig-Ladewig, L., Lin, A.M., Al-Alao, O. and Gerton, G.L. (2014) Adenine nucleotide metabolism and a role for AMP in modulating flagellar waveforms in mouse sperm. *Biol. Reprod.*, **90**, 128, 1–14.
56. Ginger, M.L., Ngazoa, E.S., Pereira, C.A., Pullen, T.J., Kabiri, M., Becker, K., Gull, K. and Steverding, D. (2005) Intracellular positioning of isoforms explains an unusually large adenylate kinase gene family in the parasite *Trypanosoma brucei*. *J. Biol. Chem.*, **280**, 11781–11789.
57. Wirschell, M., Pazour, G., Yoda, A., Hirono, M., Kamiya, R. and Witman, G.B. (2004) Oda5p, a novel axonemal protein required for assembly of the outer dynein arm and an associated adenylate kinase. *Mol. Biol. Cell*, **15**, 2729–2741.
58. Beene, D.L. and Scott, J.D. (2007) A-kinase anchoring proteins take shape. *Curr. Opin. Cell Biol.*, **19**, 192–198.
59. Xu, Z., Gong, Q., Xia, B., Groves, B., Zimmermann, M., Mugler, C., Mu, D., Matsumoto, B., Seaman, M. and Ma, D. (2009) A role of histone H3 lysine 4 methyltransferase components in endosomal trafficking. *J. Cell Biol.*, **186**, 343–353.
60. Cho, Y.-W., Hong, T., Hong, SHwa., Guo, H., Yu, H., Kim, D., Guszczynski, T., Dressler, G.R., Copeland, T.D., Kalkum, M. and Ge, K. (2007) PTIP associates with MLL3- and MLL4-containing histone H3 lysine 4 methyltransferase complex. *J. Biol. Chem.*, **282**, 20395–20406.
61. Jiang, H., Shukla, A., Wang, X., Chen, W.Y., Bernstein, B.E. and Roeder, R.G. (2011) Role for Dpy-30 in ES cell-fate specification by regulation of H3K4 methylation within bivalent domains. *Cell*, **144**, 513–525.
62. Stolc, V., Samanta, M.P., Tongprasit, W. and Marshall, W.F. (2005) Genome-wide transcriptional analysis of flagellar regeneration in *Chlamydomonas reinhardtii* identifies orthologs of ciliary disease genes. *Proc. Natl Acad. Sci. U S A*, **102**, 3703–3707.
63. Brown, P.R., Miki, K., Harper, D.B. and Eddy, E.M. (2003) A-kinase anchoring protein 4 binding proteins in the fibrous sheath of the sperm flagellum. *Biol. Reprod.*, **68**, 2241–2248.
64. Baccetti, B., Collodel, G., Estenoz, M., Manca, D., Moretti, E. and Piomboni, P. (2005) Gene deletions in an infertile man with sperm fibrous sheath dysplasia. *Hum. Reprod.*, **20**, 2790–2794.
65. Miki, K., Willis, W.D., Brown, P.R., Goulding, E.H., Fulcher, K.D. and Eddy, E.M. (2002) Targeted disruption of the Akap4 gene causes defects in sperm flagellum and motility. *Dev. Biol.*, **248**, 331–342.
66. Nakamura, K., Iitsuka, K. and Fujii, T. (1999) Adenylate kinase is tightly bound to axonemes of Tetrahymena cilia. *Comp. Biochem. Physiol. B Biochem. Mol. Biol.*, **124**, 195–199.

67. Noguchi, M., Sawada, T. and Akazawa, T. (2001) ATP-regenerating system in the cilia of Paramecium caudatum. *J Exp Biol*, **204**, 1063–1071.
68. Urbanska, P., Song, K., Joachimiak, E., Krzemien-Ojak, L., Koprowski, P., Hennessey, T., Jerka-Dziadosz, M., Fabczak, H., Gaertig, J., Nicastro, D. and Wloga, D. (2015) The CSC proteins FAP61 and FAP251 build the basal substructures of radial spoke 3 in cilia. *Mol. Biol. Cell*, **26**, 1463–1475.
69. Pigino, G. and Ishikawa, T. (2012) Axonemal radial spokes: 3D structure, function and assembly. *Bioarchitecture*, **2**, 50–58.
70. Castleman, V.H., Romio, L., Chodhari, R., Hirst, R.A., de Castro, S.C.P., Parker, K.A., Ybot-Gonzalez, P., Emes, R.D., Wilson, S.W., Wallis, C. *et al.* (2009) Mutations in radial spoke head protein genes RSPH9 and RSPH4A cause primary ciliary dyskinesia with central-microtubular-pair abnormalities. *Am. J. Hum. Genet.*, **84**, 197–209.
71. Jeanson, L., Copin, B., Papon, J.-F., Dastot-Le Moal, F., Duquesnoy, P., Montantin, G., Cadranel, J., Corvol, H., Coste, A., Désir, J. *et al.* (2015) RSPH3 mutations cause primary ciliary dyskinesia with central-complex defects and a near absence of radial spokes. *Am. J. Hum. Genet.*, **97**, 153–162.
72. Knowles, M.R., Ostrowski, L.E., Leigh, M.W., Sears, P.R., Davis, S.D., Wolf, W.E., Hazucha, M.J., Carson, J.L., Olivier, K.N., Sagel, S.D. *et al.* (2014) Mutations in RSPH1 cause primary ciliary dyskinesia with a unique clinical and ciliary phenotype. *Am. J. Respir. Crit. Care Med.*, **189**, 707–717.
73. Kott, E., Legendre, M., Copin, B., Papon, J.F., Dastot-Le Moal, F., Montantin, G., Duquesnoy, P., Piterboth, W., Amram, D., Bassinet, L. *et al.* (2013) Loss-of-function mutations in RSPH1 cause primary ciliary dyskinesia with central-complex and radial-spoke defects. *Am. J. Hum. Genet.*, **93**, 561–570.
74. El Khouri, E., Thomas, L., Jeanson, L., Bequignon, E., Vallette, B., Duquesnoy, P., Montantin, G., Copin, B., Dastot-Le Moal, F., Blanchon, S. *et al.* (2016) Mutations in DNAJB13, encoding an HSP40 family member, cause primary ciliary dyskinesia and male infertility. *Am. J. Hum. Genet.*, **99**, 489–500.
75. Inaba, K. (2003) Molecular architecture of the sperm flagella: molecules for motility and signaling. *Zoolog. Sci.*, **20**, 1043–1056.
76. Avidor-Reiss, T. and Leroux, M.R. (2015) Shared and distinct mechanisms of compartmentalized and cytosolic ciliogenesis. *Curr. Biol.*, **25**, R1143–R1150.
77. Cooper, T.G., Noonan, E., von Eckardstein, S., Auger, J., Baker, H.W., Behre, H.M., Haugen, T.B., Kruger, T., Wang, C., Mbizvo, M.T. *et al.* (2010) World Health Organization reference values for human semen characteristics. *Hum. Reprod. Update*, **16**, 231–245.
78. Auger, J., Jouannet, P. and Eustache, F. (2016) Another look at human sperm morphology. *Hum. Reprod.*, **31**, 10–23.
79. Consortium, S.M.-I. (2014) A comprehensive assessment of RNA-seq accuracy, reproducibility and information content by the Sequencing Quality Control Consortium. *Nat. Biotechnol.*, **32**, 903–914.
80. Genomes Project, C., Abecasis, G.R., Auton, A., Brooks, L.D., DePristo, M.A., Durbin, R.M., Handsaker, R.E., Kang, H.M., Marth, G.T. and McVean, G.A. (2012) An integrated map of genetic variation from 1, 092 human genomes. *Nature*, **491**, 56–65.
81. Tamalet, A., Clement, A., Roudot-Thoraval, F., Desmarquest, P., Roger, G., Boule, M., Millepied, M.C., Baculard, T.A. and Escudier, E. (2001) Abnormal central complex is a marker of severity in the presence of partial ciliary defect. *Pediatrics*, **108**, E86.
82. Papon, J.F., Bassinet, L., Cariou-Patron, G., Zerah-Lancner, F., Vojtek, A.M., Blanchon, S., Crestani, B., Amselem, S., Coste, A., Housset, B. *et al.* (2012) Quantitative analysis of ciliary beating in primary ciliary dyskinesia: a pilot study. *Orphanet J Rare Dis.*, **7**, 78.